METABOLIC DISRUPTION IMPAIRS RIBOSOMAL PROTEIN LEVELS, RESULTING IN ENHANCED AMINOGLYCOSIDE TOLERANCE

Rauf Shiraliyev and Mehmet A. Orman

William A. Brookshire Department of Chemical and Biomolecular Engineering, University of Houston, Houston, TX, 77204
Corresponding author: Mehmet Orman, morman@central.uh.edu

ABSTRACT

Aminoglycosides, a class of antibiotics, have been in use for decades, displaying broad-spectrum activity against Gram-negative and Gram-positive bacteria. They target ribosomes and disrupt protein synthesis. Although their use declined due to newer antibiotics with lower toxicity, increasing drug resistance has renewed interest in aminoglycosides. Herein, we have demonstrated that energy metabolism plays a crucial role in aminoglycoside tolerance, as knockout strains with deleted genes associated with the tricarboxylic acid cycle (TCA) and the electron transport chain (ETC) exhibited increased tolerance to aminoglycosides in the mid-exponential growth phase of *Escherichia coli* cells. Our initial hypothesis posited that genetic perturbations would lead to a reduction in the proton motive force, subsequently affecting the uptake of aminoglycosides. This hypothesis is based on the prevailing notion that aminoglycoside uptake is dependent on the distinctive and energy-driven electrochemical potential across the cytoplasmic membrane. However, our results did not support this hypothesis. Despite genetic perturbations in mutant strains, we found no consistent metabolic changes, ATP levels, cytoplasmic pH variations, or membrane potential differences compared to wild-type strains. Additionally, intracellular concentrations of fluorophore-labeled gentamicin remained similar across all strains. To uncover the mechanism responsible for the observed tolerance in mutant strains, we employed untargeted mass spectrometry to quantify the proteins within these mutants and subsequently compared them to their wild-type counterparts. Our comprehensive analysis, which encompassed protein-protein association networks and functional enrichment, unveiled a noteworthy upregulation of proteins linked to the TCA cycle in the mutant strains, suggesting that these strains compensate for the perturbation in their energy metabolism by increasing TCA cycle activity to maintain their membrane potential and ATP levels. Furthermore, our pathway enrichment analysis shed light on local network clusters displaying downregulation across all mutant strains, which were associated

with both large and small ribosomal binding proteins, ribosome biogenesis, translation factor activity, and the biosynthesis of ribonucleoside monophosphates. These findings offer a plausible explanation for the observed tolerance of aminoglycosides in the mutant strains. Altogether, this research has the potential to uncover mechanisms behind aminoglycoside tolerance, paving the way for novel strategies to combat such cells.

INTRODUCTION

Global public health is currently confronted with a critical challenge in the form of antimicrobial resistance, a threat that significantly jeopardizes human well-being (Binder et al., 1999). Addressing this escalating issue necessitates a comprehensive understanding of the diverse mechanisms employed by bacterial cells to survive antibiotic treatments. These mechanisms can be broadly classified into two groups: reversible and irreversible. Reversible mechanisms, often termed "tolerance" mechanisms, are not genetically inherited and encompass alterations in bacterial growth and behavior. Within this category, antibiotic-tolerant cells, including persisters, viable but nonculturable cells, and stationary-phase cells, exhibit the ability to transiently survive high antibiotic concentrations. Their formation is linked to stochastic and/or deterministic processes triggered by various stress factors such as the SOS response, stringent response, reactive oxygen species, nutrient depletion, and overpopulation (Amato et al., 2013; Germain et al., 2015; Molina-Quiroz et al., 2018; Theodore et al., 2013). The reversible nature of these cells allows them to oscillate between antibiotic-tolerant and sensitive states. Conversely, irreversible mechanisms, referred to as "resistance" mechanisms, are heritable and connected to mutagenic processes (Balaban et al., 2019). Antibiotic-resistant mutants, falling into this category, can emerge due to mutations in antibiotic target proteins or proteins that contribute to enhanced repair mechanisms, cell dormancy, drug efflux systems, and alternative mechanisms that circumvent the antibiotic's target (Lambert, 2005; Okusu et al., 1996).

Aminoglycosides, having received approval for human use, were among the earliest antibiotics to be used in clinical practice (Becker and Cooper, 2013; Krause et al., 2016). Aminoglycosides are a class of naturally occurring or semisynthetic amino-modified sugars known for their broad-spectrum activity against both Gram-negative and Gram-positive bacteria (Aggen et al., 2010; Endimiani et al., 2009; Landman et al., 2010; Ristuccia and Cunha, 1985). They have been a crucial

62 part of antibacterial therapy since the discovery and introduction of streptomycin for the treatment
63 of tuberculosis, which was isolated from the soil bacterium *Streptomyces griseus* (Kresge et al.,
64 2004; Schatz et al., 2005; Woodruff, 2014). This was followed by the emergence of other members
65 of the class, including gentamicin, kanamycin, tobramycin, amikacin, and neomycin (Becker and
66 Cooper, 2013; Krause et al., 2016). The use of aminoglycosides declined with the advent of newer
67 antibiotics, such as fluoroquinolones, which were thought to have lower toxicity (Becker and
68 Cooper, 2013; Krause et al., 2016). However, the rise of resistance to these drug classes has
69 sparked a revival of interest in the older aminoglycosides and the development of new ones with
70 improved dosing schemes (Becker and Cooper, 2013; Krause et al., 2016).

71 Studies on the mechanism of action of aminoglycosides against bacteria have shown that they
72 disrupt protein synthesis by targeting the ribosome. The primary action of aminoglycosides is to
73 bind to the 16S ribosomal RNA (rRNA) of bacteria, a component of the 30S ribosomal subunit
74 (Moazed and Noller, 1987; Recht et al., 1999; Woodcock et al., 1991). The initial entry of
75 antibiotics into cells causes misreading as the antibiotics interact with the ribosomes involved in
76 chain elongation. This is the first step in bactericidal action. Following this, the misread protein is
77 incorporated into the membrane, causing membrane damage (Davis et al., 1986). This increases
78 the amount of antibiotics entering the cells, leading to more misreading and the formation of
79 channels (Davis et al., 1986). Finally, the blockage of the initiating ribosomes occurs, causing the
80 inhibition of protein synthesis (Davis et al., 1986). Aminoglycosides can also bind to and stabilize
81 RNA helix 69 (H69) of 50S ribosomal subunit, potentially inhibiting ribosome recycling facilitated
82 by ribosome recycling factor (Borovinskaya et al., 2007). Moreover, the binding of
83 aminoglycosides to the 50S ribosomal subunit can lead to the inhibition of mRNA and tRNA
84 translocation (Borovinskaya et al., 2007).

85 It has been demonstrated that antibiotic-tolerant cells can become susceptible to aminoglycosides
86 by metabolizing certain carbon sources (Allison et al., 2011). This susceptibility arises from an
87 enhanced drug uptake as a result of an increase in the electron transport chain activity and
88 membrane potential, facilitated by the breakdown of these specific carbon sources (Allison et al.,
89 2011). The process of aminoglycoside uptake is considered to be a unique, energy-requiring
90 mechanism where the electrochemical potential across the cytoplasmic membrane and electron
91 flow through membrane-bound respiratory chains are believed to be significant factors (Taber
92 Harry W et al., 1987). However, the bactericidal effect of aminoglycosides may not result from

93 the downstream impacts of voltage-dependent drug uptake, but rather from an irregular membrane
94 potential (Bruni and Kralj, 2020). Bruni and Kralj suggested that hyperpolarization, stemming
95 from changes in ATP flux due to the reversal of F1Fo-ATPase activity, could potentially intensify
96 aminoglycoside-mediated cell death (Bruni and Kralj, 2020).

97 While a renewed interest in aminoglycoside antibiotics has unveiled interesting connections
98 between bacterial energy metabolism and aminoglycoside tolerance, the precise impact of energy
99 metabolism disruption on energy-dependent aminoglycoside uptake remains unclear. In our study,
100 we found that knockout strains with genes related to the tricarboxylic acid cycle (TCA) and the
101 electron transport chain (ETC) deleted displayed increased tolerance to aminoglycosides.
102 Intriguingly, this increased tolerance was not attributed to reduced proton motive force, which
103 affects drug uptake, as evidenced by insignificant alterations in ATP levels or membrane potential
104 compared to the wild-type strain. We employed untargeted mass spectrometry to quantify proteins
105 in the mutant and wild-type strains, revealing a notable upregulation of proteins associated with
106 the TCA cycle in the mutants. This suggests that these strains compensate for the disruption in
107 their energy metabolism by enhancing TCA cycle activity to maintain their membrane potential
108 and ATP levels. Moreover, our pathway enrichment analysis emphasized local network clusters
109 that were consistently downregulated across all mutant strains. These clusters were related to both
110 large and small ribosomal binding proteins, ribosome biogenesis, translation factor activity, and
111 the biosynthesis of ribonucleoside monophosphates. These findings provide a credible rationale
112 for the observed tolerance to aminoglycosides in the mutant strains.

113

114 **RESULTS**

115 **Deletions of the TCA cycle and ETC genes increased tolerance to aminoglycosides.**

116 Given the crucial role of energy metabolism in aminoglycoside tolerance, our initial objective was
117 to assess various knockout strains that involved the deletion of genes associated with the TCA
118 cycle, such as *sucA, gltA, mdh, sdhC, icd, acnB,* and *fumA,* as well as the NADH dehydrogenase
119 enzyme of ETC, including *nuoM* and *nuoI* from *E. coli* MG1655. To conduct the experiments,
120 both wild-type and mutant strains were cultured overnight and then diluted 100-fold in fresh Luria-
121 Bertani (LB) medium. The cultures were grown until the mid-exponential phase (t=3.5 hours) in a
122 shaker at 37°C and 250 rpm. Subsequently, the cultures were exposed to various aminoglycosides

(50 μg/ml streptomycin, 50 μg/ml gentamicin, and 50 μg/ml amikacin) for a duration of 5 hours. Samples were collected before and after the treatments, and these were plated on LB agar to quantify the surviving cell fractions. Analysis of the results indicates that most of the knockout strains (Δ*sucA,* Δ*gltA,* Δ*mdh,* Δ*sdhC,* Δ*nuoM,* and Δ*nuoI*) exhibited increased tolerance to streptomycin, gentamicin, and amikacin treatments when compared to the wild-type strain (**Figure 1A-C**). However, it is worth noting that mutant strains such as Δ*icd,* Δ*acnB,* and Δ*fumA* did not always exhibit increased tolerance (**Figure 1A-C**), underscoring the complex interplay between energy metabolism and specific antibiotic tolerance. Moreover, the surviving cells measured in these assays may not necessarily represent antibiotic-resistant cells, as the antibiotic tolerance assays were conducted at concentrations well above the Minimum Inhibitory Concentration (MIC) levels. The MIC levels of the strains for the tested antibiotics displayed no drastic alterations compared to those of the wild type, despite some minor variations among them (**Supplementary Table S1**).

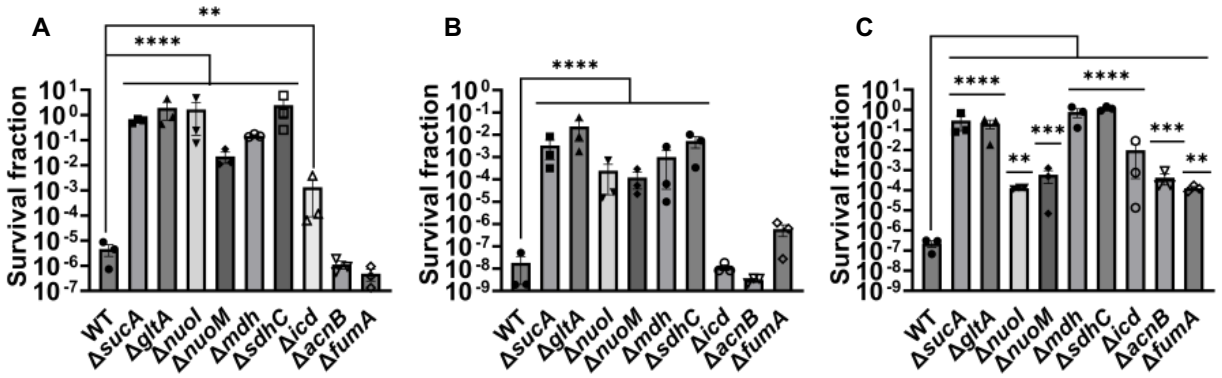

Figure 1. Deletions in the TCA cycle and ETC genes enhance tolerance to aminoglycosides. In the mid-exponential phase (t=3.5 h), *E. coli* MG1655 wild-type and knockout strains underwent (A) streptomycin, (B) gentamicin, and (C) amikacin treatments at a concentration of 50 μg/ml for a duration of 5 hours. Following the treatments, cells were washed to eliminate the antibiotics and then plated on LB agar plates to quantify the surviving cell fractions. CFU: Colony forming units. WT: Wild type. For pairwise comparisons, one-way ANOVA with Dunnett's post hoc test was used where *, $P < 0.05$, **, $P < 0.01$, ***, $P < 0.001$, and ****, $P < 0.0001$. N=3. Data points represent mean and standard error.

To gain a thorough understanding of the observed tolerance, we chose four mutant strains that exhibit either high tolerance (*sucA, gltA,* and *nuoI*) or low tolerance (*icd*) to gentamicin for the subsequent assays. Our initial objective was to delineate the time-dependent profiles of antibiotic-tolerant cells within cultures. To achieve this, cells from overnight cultures were diluted in fresh

149 media and cultured for 6 hours. Hourly samples were collected for cell quantification and antibiotic
150 tolerance assays. We opted for flow cytometry for precise cell quantification, a more reliable
151 method than optical density measurements (Mohiuddin et al., 2020) (**Figure 2A**). In the antibiotic
152 tolerance assays, samples were treated with gentamicin (50 µg/ml) for 5 hours and plated before
153 and after the treatments (**Figure 2B**). Notably, the observed tolerance in these mutant strains is not
154 linked to cell growth. For instance, the mutant strains associated with *sucA, gltA,* and *nuoI* genes
155 exhibited higher tolerance to aminoglycosides although they did not show significantly altered cell
156 growth compared to the wild type (**Figure 2A, B**). Notably, these mutant strains displayed a
157 substantial increase in the number of tolerant cells (more than 10^4-fold) between time points t=3
158 and t=4 hours during the mid-exponential growth phase when compared to the wild-type strain
159 (**Figure 2B**). Conversely, while the *icd* mutant exhibited a significant reduction in cell growth, it
160 was observed to be as sensitive to aminoglycosides as the wild type during the exponential growth
161 phase and the formation of tolerant cells in this mutant strain was only evident after the time point
162 t=5 hours (**Figure 2A, B**). We also emphasize that the observed tolerance in the mutant strains is
163 transient or reversible, as they all exhibit high sensitivity to aminoglycosides, similar to the wild
164 type, during the lag phase of growth (**Figure 2B**).

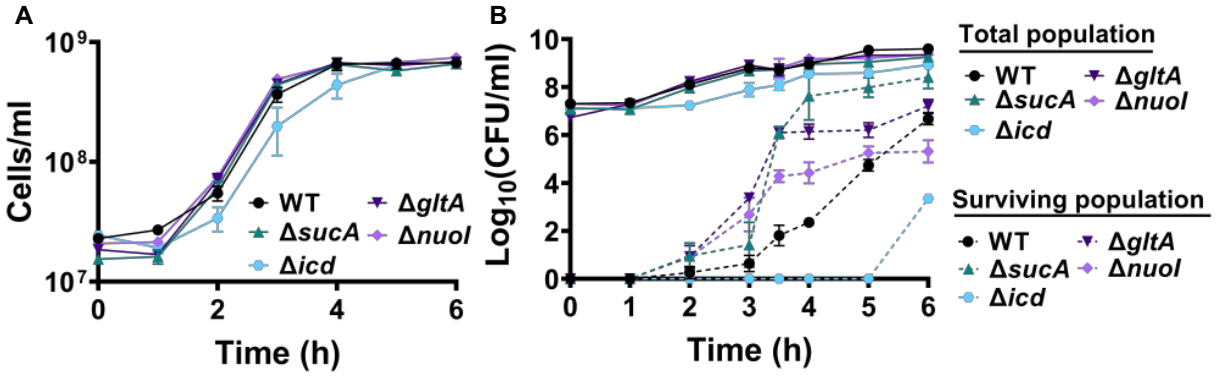

165

166 **Figure 2. The observed tolerance in the mutant strains is not linked to cell growth.** (A) Growth of *E.*
167 *coli* MG1655 wild type, Δ*sucA*, Δ*gltA*, Δ*nuoI*, and Δ*icd* strains was assessed by measuring the number of
168 cells per ml with flow cytometry. (B) The cells of both the *E. coli* MG1655 WT and mutant strains were
169 collected from the cultures at indicated time intervals and then subjected to gentamicin treatment. The figure
170 shows the colony-forming unit (CFU) levels of both the treated and untreated cultures, indicating the
171 surviving and total cell population, respectively. N=3. Data points represent mean and standard error.

172

173 **Energy-dependent aminoglycoside uptake is not a contributing factor.**

174 Aminoglycoside uptake is a unique and energy-requiring mechanism that depends on the

175 electrochemical potential across the cytoplasmic membrane (Taber Harry W et al., 1987). Initially,
176 we hypothesized that the genetic perturbations in these strains may have decreased PMF and
177 aminoglycoside uptake. The mutant strains exhibiting increased aminoglycoside tolerance
178 demonstrated no consistent pattern in metabolic activities during the mid-exponential growth
179 phase, which was assessed using redox sensor green (RSG) dye for the indicated time points (t=3,
180 4, 5 and 6 hours) of the cell growth (**Figure 3A**). RSG dye can be reduced by bacterial reductases
181 of PMF, allowing it to enter the bacteria and produce a green fluorescence signal. This fluorescence
182 signal should be suppressed by the presence of a metabolic inhibitor, such as carbonyl cyanide 3-
183 chlorophenylhydrazone (CCCP) (**Supplementary Figure S1**). Given that ATP is a pivotal product
184 of PMF, we also quantified intracellular ATP levels in both wildtype and mutant strains, employing
185 the BacTiter-Glo™ Microbial Cell Viability Assay (Catalog# G8230, Promega Corporation,
186 Madison WI). This assay utilizes a single reagent to lyse cells and produce luminescence through
187 the luciferase reaction, with the luminescent signal being directly proportional to the ATP content
188 (**Supplementary Figure S2**). We found no consistent pattern in ATP levels between the antibiotic-
189 sensitive and tolerant strains, particularly during the mid-exponential growth phase (at t=3 and 4
190 hours) (**Figure 3B**). While the Δ*sucA* mutant generally showed reduced ATP levels, this was not
191 the case for the other strains, which showed increased ATP levels around t=6 hours (**Figure 3B**).

192

193 Furthermore, since the proton gradient is a vital element of PMF and a reduced H^+ ion gradient
194 across the cell membrane is linked to reduced membrane potential, we conducted measurements
195 of intracellular pH using the ratiometric pHluorin, known as a pH-sensitive derivative of green
196 fluorescent protein (GFP) (Miesenböck et al., 1998). This GFP variant exhibits a bimodal
197 excitation spectrum characterized by peaks at 410 nm and 470 nm, along with an emission
198 maximum at 530 nm (Martinez II et al., 2012). When subjected to acidification, the excitation at
199 410 nm diminishes while the excitation at 470 nm concurrently rises, which allows us to construct
200 standard curves for the measurement of intracellular pH (**Supplementary Figure S3**). For these
201 assessments, we introduced pGFPR01 plasmids, where pHluorin is expressed under the arabinose-
202 induced promoter PBAD, into the mutant strains utilized. Our results revealed that there was no
203 anticipated acidification of the cytoplasm in the TCA and ETC mutants compared to the wild type,
204 both during the mid-exponential and early stationary phases (**Figure 3C**).

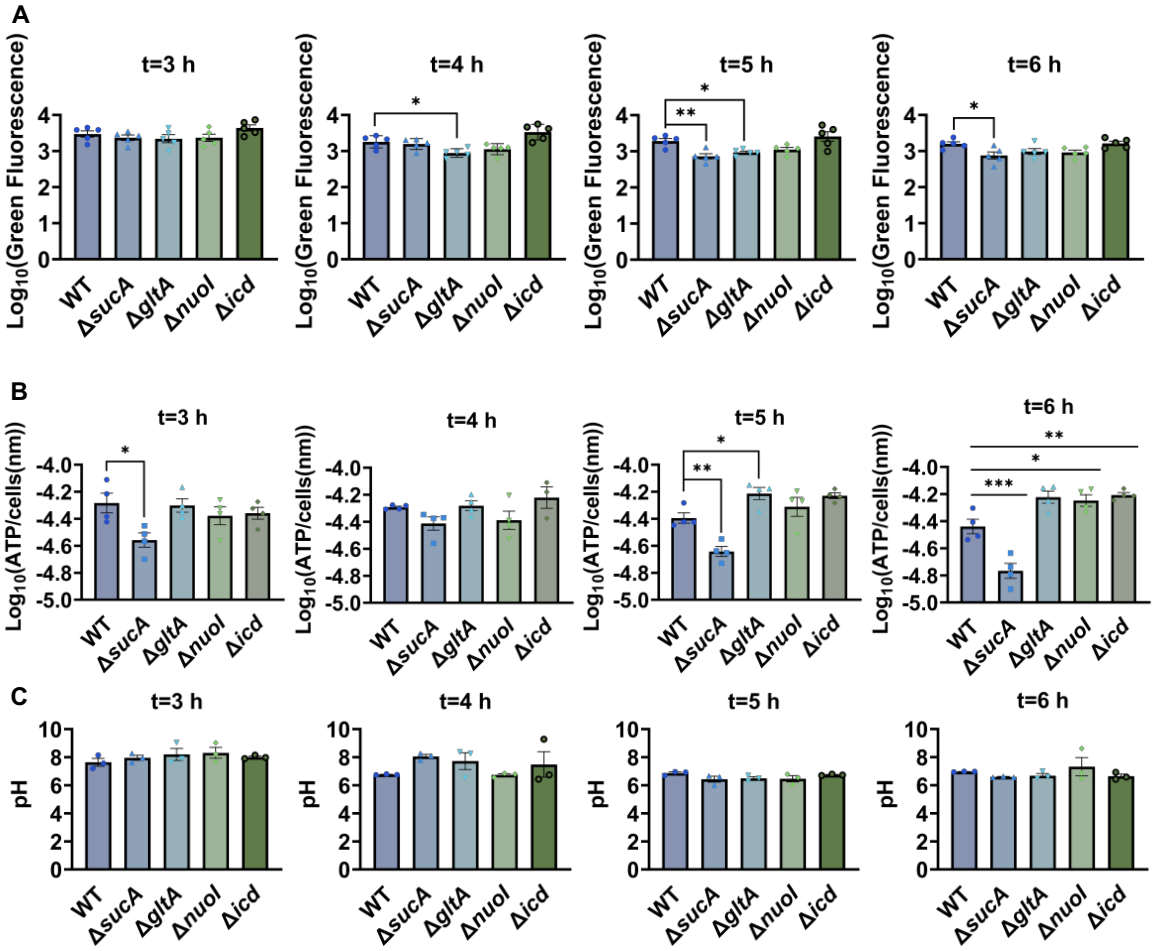

Figure 3. Comparable ATP levels, redox activities, and cytoplasmic pH levels were observed between the wild-type and mutant strains. (A) RSG staining was conducted by suspending wild-type and mutant strains in 0.85% sodium chloride solution during the mid-exponential and early stationary phases, as outlined in the Materials and Methods section. (B) The ATP levels were measured in wild type and mutant cells during the mid-exponential and early stationary growth phases. (C) Comparison of the cytoplasmic pH of the WT and mutant cells during the mid-exponential and stationary phases was performed using using the ratiometric pHluorin. For pairwise comparisons, one-way ANOVA with Dunnett's post hoc test was used where *, $P < 0.05$, **, $P < 0.01$, ***, and $P < 0.001$. $N \geq 3$. Data points represent mean and standard error.

Finally, we utilized fluorophore-labeled aminoglycoside (Gentamicin-Texas Red, or GTTR) to investigate the cellular uptake of the drug. Specifically, cells in the mid-exponential phase of both wild-type and mutant strains (at t=3.5 hours when a significant increase in gentamicin tolerance was observed in the mutant strains) were exposed to GTTR for an hour, followed by the analysis of cells using flow cytometry. A short-term treatment was preferred, in line with a previous study (Bruni and Kralj, 2020) as cells treated with aminoglycosides become permeabilized at later time

222 points (Bruni and Kralj, 2020), potentially introducing artificial impacts on drug uptake. Notably,
223 the deletion of genes related to the TCA cycle and the electron transport chain did not induce a
224 significant alteration in GTTR uptake in cells during the exponential phase when compared to the
225 wild type (**Figure 4A, B**). Collectively, these findings from multiple approaches strongly suggest
226 that energy-dependent drug uptake is not the primary determinant of the observed antibiotic
227 tolerance.

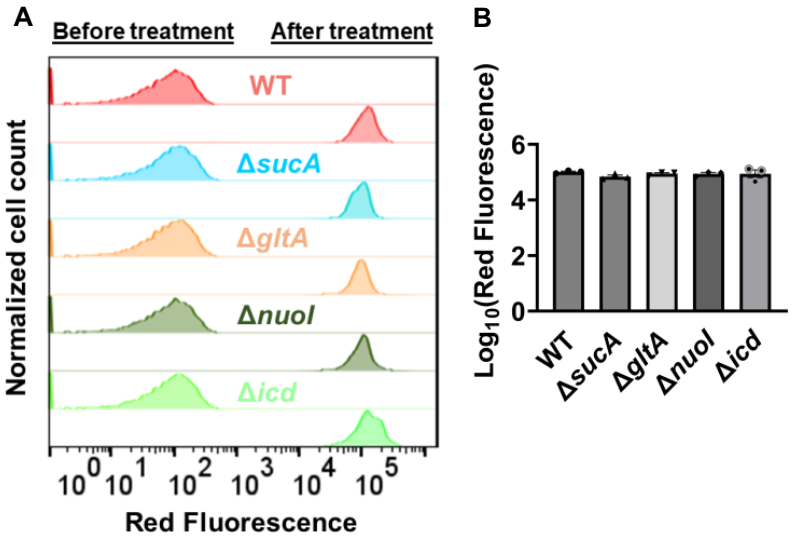

228

229 **Figure 4. Deletion of genes associated with the TCA cycle and electron transport chain showed no**
230 **significant alteration in drug uptake.** (A) Exemplary quantification of gentamicin-Texas red uptake in
231 cells during the exponential growth phase. (B) Gentamicin-Texas red staining was performed on cells in
232 the mid-exponential phase for both the wild-type and mutant strains, followed by fluorescence measurement
233 using flow cytometry after one hour. For pairwise comparisons, one-way ANOVA with Dunnett's post hoc
234 test was used (no statistical significance was detected). N=3. Data points represent mean and standard error.

235

236 **Membrane potential dysregulation is not associated with the observed aminoglycoside**
237 **tolerance.**

238 Fluorescent sensors for voltage and calcium have been utilized to monitor electrophysiology in
239 bacteria at the single-cell level (Bruni and Kralj, 2020), and the findings revealed that the
240 dysregulated membrane voltage was not essential for aminoglycoside uptake or inner membrane
241 pore formation in *E. coli*, but it proved crucial for bactericidal activity (Bruni and Kralj, 2020). To
242 assess the significance of dysregulated PMF, we employed a well-established assay based on 3,3′-
243 Dipropylthiadicarbocyanine [$DiSC_3(5)$] (Stokes et al., 2020; Wu et al., 1999), a fluorescent dye
244 commonly used for monitoring cell membrane potential. During cell hyperpolarization, $DiSC_3(5)$

245 infiltrates the cell membrane, undergoing self-quenching and resulting in reduced fluorescence
246 intensity. Conversely, during depolarization, the fluorescence intensity of $DiSC_3(5)$ increases as it
247 exits the cell membrane. Polymyxin B served as a control (**Supplementary Figure S4**), as the
248 polycationic peptide ring of polymyxin B binds to a negatively charged site within the
249 lipopolysaccharide layer of the cellular membrane (Domingues et al., 2012), leading to the
250 dissipation of the electric potential gradient which enhances the fluorescence intensity of $DiSC_3(5)$
251 (**Supplementary Figure S4**). To assess the effect of gentamicin on membrane potential,
252 metabolically active cells from exponential phase cultures at time points t=3, 4, 5, and 6 hours
253 were transferred to a buffer solution containing 1 μM $DiSC_3(5)$ (**Figure 5**). Upon reaching
254 equilibrium, the cells were treated with gentamicin. At designated time points, samples were
255 collected, and fluorescence levels were measured using a plate reader (**Figure 5**). Similar to
256 Polymyxin B treatments, gentamicin disrupts the electric potential gradient of PMF, leading to an
257 increase in the fluorescence intensity of $DiSC_3(5)$ (**Figure 5**). Despite significant and rapid
258 alterations in membrane potential observed upon gentamicin treatment, there was no significant
259 difference in membrane potential between aminoglycoside-sensitive and tolerant strains (**Figure**
260 **5**). Moreover, if any of the gene deletions had an impact on membrane potential, we would have
261 expected to observe altered fluorescence intensity in the specific knockout strain compared to that
262 of the wild type during the equilibrium stage (before the addition of the drug), as previously
263 reported (Mohiuddin et al., 2022). However, no significant difference in $DiSC_3(5)$ fluorescence
264 intensities was observed among the strains tested during the equilibrium phase (the initial 20
265 minutes, as illustrated in **Figure 5**).

266 The membrane dysregulation induced by aminoglycosides was previously attributed to the
267 combined activity of NADH dehydrogenase and a reversed F1Fo-ATPase (Bruni and Kralj, 2020),
268 and the knockout strains targeting the proton-conducting Fo domain (Δ*atpB,* Δ*atpE,* Δ*atpF*), as
269 well as Δ*atpG*, showed increased colony-forming units in response to aminoglycoside treatments
270 (Bruni and Kralj, 2020). However, when we tested ATP synthase knockout strains of *E. coli*
271 BW25113 from the Keio collection (for consistency with the previous study (Bruni and Kralj,
272 2020)), we did not observe a comparable trend as reported earlier (Bruni and Kralj, 2020). In fact,
273 the strains Δ*atpB,* Δ*atpE,* Δ*atpF,* and Δ*atpG* exhibited similar sensitivity to gentamicin compared
274 to the wild type under the conditions studied here (**Supplementary Figure S5A**). Interestingly,
275 we observed a drastic increase in gentamicin tolerance in the Δ*atpC* mutant strain (**Supplementary**

276 **Figure S5A**), which was not reported in the previous study (Bruni and Kralj, 2020). The *atpC* gene
277 encodes an F1 complex subunit of ATP synthase, promoting motor activity in the direction of ATP
278 production rather than the reversed direction (Bruni and Kralj, 2020; Guo et al., 2019). We
279 acknowledge potential variations between *E. coli* BW25113 and *E. coli* MG1655 strains, due to
280 differences in their genomic DNA. To address this, we deleted two Fo components (Δ*atpA* and
281 Δ*atpB*) and two F1 components (Δ*atpC* and Δ*atpD*) from *E. coli* MG1655 and assessed their
282 gentamicin survival profiles. Notably, the drastic increase in the number of tolerant cells reported
283 for the TCA and ETC mutant strains during the mid-exponential growth phase was not observed
284 in these ATP synthase mutant strains. However, a moderate increase in tolerance was noted for
285 the Δ*atpC* and Δ*atpD* mutants (F1 components) during the mid-exponential phase (t=3 and 4
286 hours) compared to the wild type (**Supplementary Figure S5B**), without a clear trend supporting
287 a reverse ATPase-mediated killing through the Fo domain. Overall, while we observe gentamicin-
288 induced dysregulation in membrane potential, it may not be the primary factor contributing to the
289 observed differences in antibiotic tolerance levels between the strains.

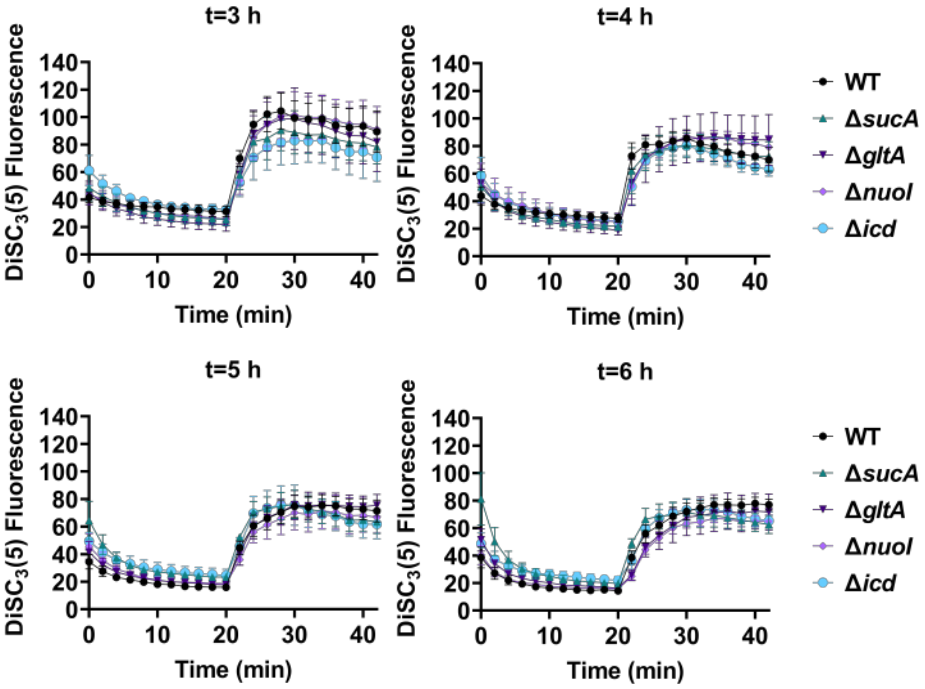

290

291 **Figure 5. The dysregulation of membrane potential is not correlated with the observed**
292 **aminoglycoside tolerance.** Deletion of TCA cycle and electron transport chain involved strains showed no
293 significant change in PMF. Mid-exponential and early stationary phase cells of wild type and mutant strains
294 were stained with $DiSC_3(5)$, and at specified time intervals their fluorescence was measured using a plate
295 reader. Cells were treated with gentamicin after 20 minutes and fluorescence was measured again. N=4.
296 Data points represent mean and standard error.

297 **Proteomic analysis reveals molecular responses in mutant strains, unveiling potential**
298 **mechanisms underlying aminoglycoside tolerance.**

299 In order to gain further insights beyond the conducted experiments and elucidate the mechanism
300 responsible for the observed tolerance in TCA cycle and ETC mutants, we utilized untargeted mass
301 spectrometry to quantify proteins within these mutants and subsequently compared them to their
302 wild-type counterparts. Proteomics data analysis, specifically involving the determination of
303 protein fold-change and calculation of P-value (using *F*-test and *t*-test), was carried out through a
304 structured process involving data transformation, normalization, and statistical procedures, as
305 detailed elsewhere (Aguilan et al., 2020). Proteins exhibiting a positive $\log_2$(fold-change) and a P-
306 value less than 0.05 were categorized as significantly upregulated, while those displaying a
307 negative $\log_2$(fold-change) and a P-value less than 0.05 were categorized as significantly
308 downregulated. The STRING database was employed to predict both the physical and functional
309 interactions between proteins by entering a group of upregulated and downregulated proteins
310 (Szklarczyk et al., 2023). Additionally, STRING carried out an automated pathway-enrichment
311 analysis, focusing on the proteins entered and identifying pathways that occurred more frequently
312 than expected. The analysis was based on the statistical background of the entire genome and
313 encompassed Gene Ontology annotations (all three domains), KEGG pathways, Uniprot
314 keywords, and other functional pathway classification frameworks. This also included a
315 hierarchical clustering of the STRING network itself. When discussing our findings, we primarily
316 reference the latter method, as it offers the advantage of broader coverage, including potential
317 novel modules that might not yet be classified as pathways (Szklarczyk et al., 2019).

318 In the context of the upregulated protein-protein association networks in the Δ*sucA* and Δ*gltA*
319 mutant strains, the STRING analysis unveiled significant functional enrichments (**Supplementary**
320 **Table S2 and S3**). These included the TCA cycle, carbon and pyruvate metabolism, formate c-
321 acetyltransferase activity, and the fatty acid metabolic pathway (**Figure 6A, B, D, and E**).
322 Specifically, key proteins associated with these enrichments encompassed FumA, FumC, AcnA,
323 AcnB, SdhA, SdhB, Dld, TalA, FbaB, FadA, FadB, and Acs (**Figure 6A, B**). Additionally, the
324 Δ*sucA* and Δ*gltA* mutants exhibited an upregulated cluster of membrane proteins, particularly from
325 the ABC transporter family (MalK, RbsA, RbsB, DppA, OppA, UgpB, LuxS), with some proteins
326 specialized in amino acid transport across the plasma membrane (ArtL, LivJ, GltI, GlnQ, ArgT,
327 HisJ) (**Figure 6A, B**). In the case of the Δ*gltA* mutant, a smaller network of upregulated stress-

328 induced proteins was also observed, related to osmotic stress, oxidative stress, and starvation
329 (OsmC, OsmY, YbaY, YgaU, YjbJ, Dps, WrbA) (**Figure 6B**). Regarding the Δ*nuoI* mutant, the
330 STRING analysis identified an upregulated functional network associated with carbon and
331 pyruvate metabolism, featuring proteins SucD, FumA, SdhA, Crp, Eda, GalS, Crr, Mdh, PykF,
332 Lpd, GapA, Pgk, PoxB, and TalA, as well as upregulated flagellar proteins (FlgF, FlgK, FlgM,
333 FliD, FliH, FliJ, FliK, FliN, CheW) (**Figure 6C, F, Supplementary Table S4**). Interestingly, our
334 proteomics data on these three mutant strains, which display higher gentamicin tolerance, reveals
335 upregulation in proteins associated with energy metabolism (e.g., TCA cycle, pyruvate
336 metabolism) (**Figure 6**). This suggests that these mutant strains compensate for metabolic
337 perturbations by enhancing the TCA cycle to preserve their ATP levels, redox activities, and PMF.
338 Indeed, this proteomics data aligns well with measurements of ATP, RSG, and PMF highlighted
339 in previous sections (**Figures 3-5**).

340 In the context of downregulated protein networks, the substantial functional enrichments unveiled
341 through analysis using the STRING database were found to be intricately associated with both the
342 large and small ribosomal subunits, denoted by the specific ribosomal proteins Rplx, Rplm, Rplt,
343 Rply, Rplp, Rpls, Rpse, Rpsg, Rpsh, Rpsm, Rpst, Rpsi, Rpsp, Rpsk, Rpsc, Rpsd, Rpsl, Rpmg,
344 Rpmf, and Rpmb (**Supplementary Table S5, S6, and S7, Figure 7A-F**). These enrichments
345 extended to domains encompassing translation factor activities, translation processes, and protein
346 export mechanisms, featuring genes Rimm, Infa, Infc, Tsf, Yeip, Nusg, Efp, Prfc, Mfd, Glys, Cyss,
347 Asps, Args, and Tig (**Figure 7A-C**). Additionally, a noteworthy connection was established with
348 the ribonucleoside monophosphate biosynthetic process, as characterized by genes Cara, Carb,
349 Pyrd, Pyrf, and Pyrl (**Figure 7A-C**). The consistent downregulation of ribosomal binding proteins,
350 ribosome biogenesis, translation factor activity, and the biosynthesis of ribonucleoside
351 monophosphates is observed in the three mutant strains (Δ*sucA*, Δ*gltA*, and Δ*nuoI*), providing an
352 explanation for the observed aminoglycoside tolerance in these mutants (**Figure 7A-F**). However,
353 genome-level proteomics trends, specifically the upregulation in energy metabolism and
354 downregulation in ribosomal proteins, were not observed in the Δ*icd* mutant strain
355 (**Supplementary Table S8 and S9, Supplementary Figure S6**). This may be expected, as the
356 Δ*icd* mutant strain did not exhibit a significant difference in gentamicin tolerance compared to the
357 wild type.

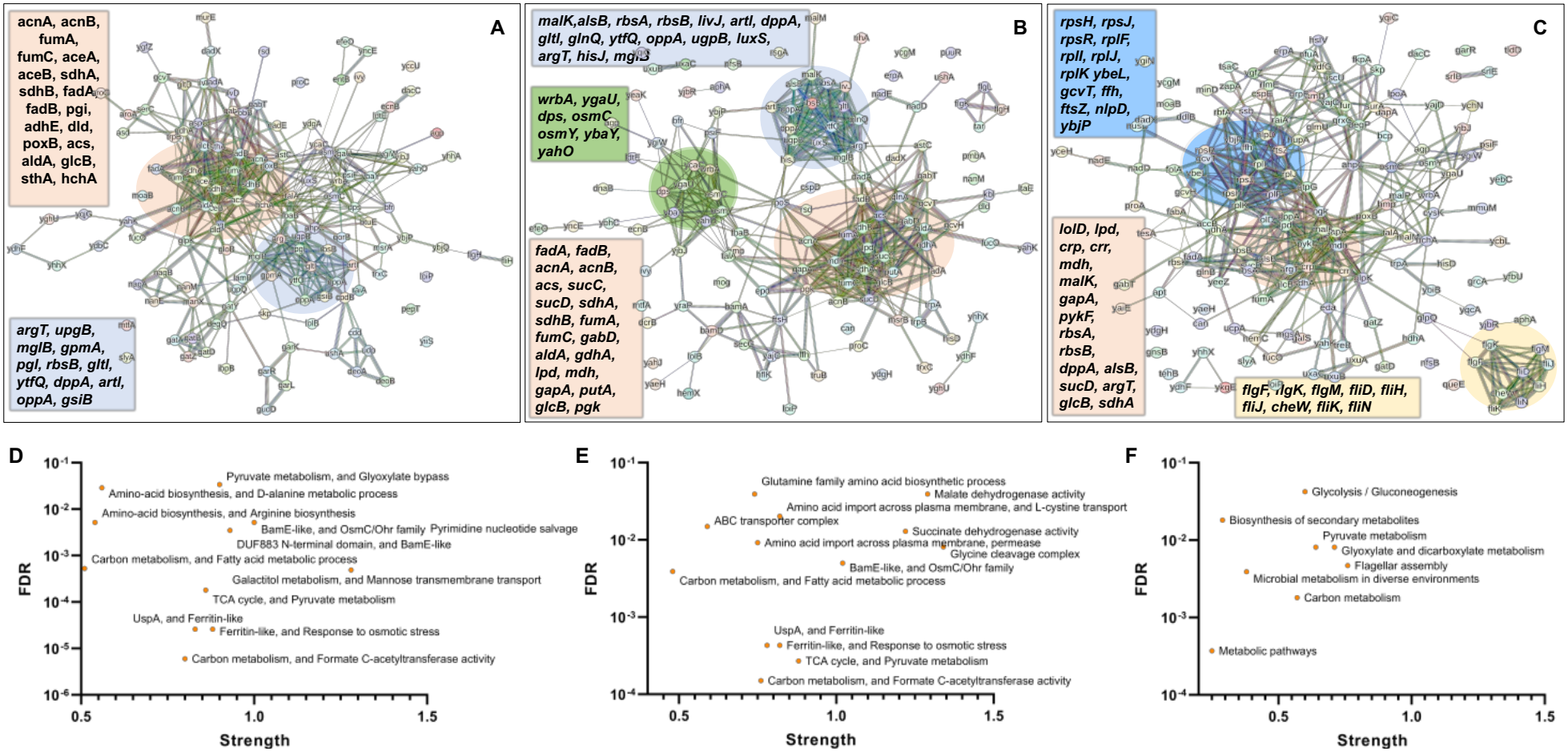

Figure 6. Proteomics data on the mutant strains, exhibiting increased gentamicin tolerance, indicates upregulation in proteins linked to energy metabolism. Cells from both wild-type and mutant strains at the mid-exponential phase (t=3.5 h) were collected after which protein extraction and digestion were carried out for Liquid Chromatography–Mass Spectrometry (LC-MS) analysis. The STRING visual network depicts upregulated protein interactions of Δ*sucA* (A), Δ*gltA* (B) and Δ*nuoI* (C) mutants. The thickness of edges in the network reflects the strength of data support, derived from curated databases, experimental data, gene neighborhood, gene fusions, co-occurrence, co-expression, protein homology, and text mining. The protein clusters and their corresponding gene names are visually distinguished through color-coding on the networks. The panels D-F depict functional enrichments in the protein network for Δ*sucA* (D), Δ*gltA* (E), and Δ*nuoI* (F) mutants. This includes information on the number of proteins associated with the enrichment strength and the false discovery rate (FDR) indicating the significance of enrichment through P-value (calculated using the Benjamini-Hochberg method). N= 3.

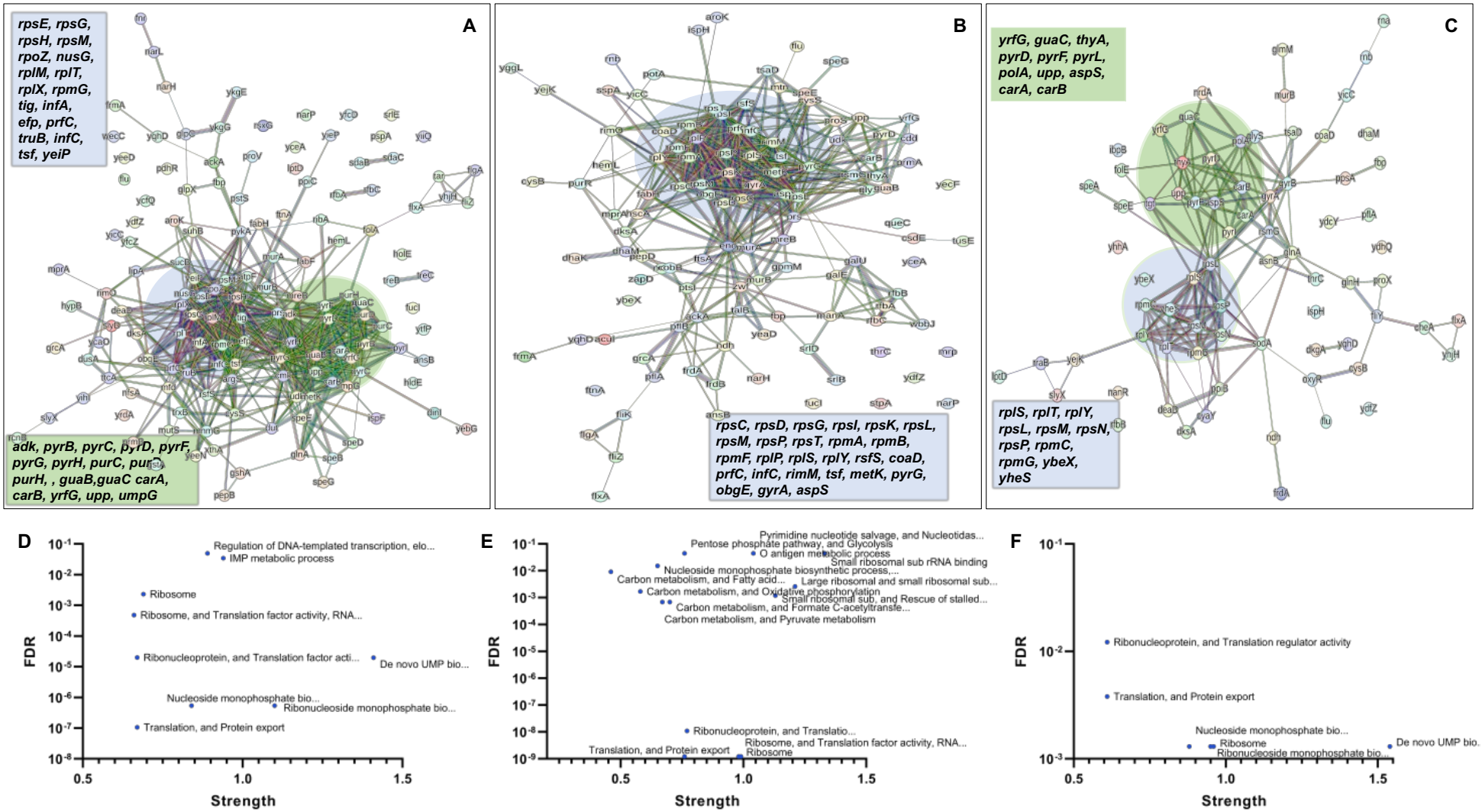

Figure 7. Proteomics data on the mutant strains, exhibiting increased gentamicin tolerance, reveals downregulation in proteins associated with ribosomes. The STRING visual network displays upregulated protein interactions for Δ*sucA* (A), Δ*gltA* (B), and Δ*nuoI* (C) mutants. Panels D-F provide details on functional enrichments in the protein network for Δ*sucA* (D), Δ*gltA* (E), and Δ*nuoI* (F) mutants. N= 3.

360 **DISCUSSION**

361 The study aimed to explore the impact of gene knockouts associated with the TCA cycle and
362 NADH dehydrogenase enzyme on aminoglycoside tolerance in *E. coli* MG1655. Various knockout
363 strains showed increased tolerance to streptomycin, gentamicin, and amikacin compared to the
364 wild-type strain. However, mutants like Δ*icd*, Δ*acnB*, and Δ*fumA* did not consistently exhibit
365 enhanced tolerance, highlighting the complex relationship between energy metabolism and
366 antibiotic tolerance. The investigation further focused on four selected mutant strains (*sucA, gltA,*
367 *nuoI,* and *icd*), revealing time-dependent profiles of antibiotic-tolerant cells, with a substantial
368 increase observed in the Δ*sucA,* Δ*gltA, and* Δ*nuoI* mutants during the mid-exponential growth
369 phase. The observed tolerance was not linked to altered cell growth, and it appeared to be transient
370 or reversible, as all mutants regained sensitivity to aminoglycosides during the lag phase of growth.

371 We further investigated the factors influencing aminoglycoside tolerance in *E. coli* MG1655 by
372 examining the role of energy-dependent drug uptake, membrane potential, and genetic
373 perturbations. Studies have shown that cells tolerant to antibiotics can transition to susceptibility
374 to aminoglycosides through the metabolism of specific carbon sources (Allison et al., 2011). This
375 shift in susceptibility is attributed to increased drug uptake, facilitated by increased activity in the
376 electron transport chain and membrane potential, both triggered by the breakdown of these
377 particular carbon sources (Allison et al., 2011). Aminoglycoside uptake involves a three-step
378 process: initial ionic binding to cells, followed by two energy-dependent phases (EDP I and EDP
379 II) (Taber Harry W et al., 1987). The first step, concentration-dependent ionic binding, is not
380 affected by inhibitors of energized uptake (Taber Harry W et al., 1987). The EDP I phase is
381 gradual, requiring aminoglycoside concentration and a membrane potential for substantial uptake
382 (Taber Harry W et al., 1987). Elevated aminoglycoside concentrations can bypass EDP I. EDP II
383 involves rapid transport across the cytoplasmic membrane, relying on energy from electron
384 transport and potentially ATP hydrolysis. Once inside the cell, studies suggest bactericidal effects
385 through mistranslation and misfolding of membrane proteins, triggering oxidative stress and
386 hydroxyl radical formation, ultimately leading to cell death (Kohanski et al., 2008, 2007). Despite
387 hypothesizing that reduced PMF and aminoglycoside uptake might be linked to genetic
388 perturbations, the mutant strains with increased tolerance showed no consistent pattern in
389 metabolic activities in our study. Analysis of ATP levels, intracellular pH, and fluorophore-labeled
390 aminoglycoside uptake did not reveal a clear association with antibiotic tolerance. Certainly, our

391 proteomic analysis revealed significant enhancements in upregulated protein networks linked to
392 the TCA cycle, carbon metabolism, pyruvate metabolism, and fatty acid pathways in the mutant
393 strains exhibiting increased gentamicin tolerance. This sheds light on how these mutants manage
394 and maintain their ATP levels, redox activities, proton motive force (PMF), and drug uptake,
395 overcoming genetic disruptions in their metabolism.

396 Bruni and Kralj postulated that the bactericidal action triggered by membrane potential might
397 involve mechanisms beyond drug uptake, potentially influenced by the combined effects of pore
398 formation by mistranslated proteins and membrane hyperpolarization (Bruni and Kralj, 2020).
399 Additionally, their study proposed that the sudden shift in energy demand resulting from ribosome
400 dissociation during aminoglycoside treatment could boost cellular ATP flux, leading to
401 hyperpolarization through the concerted activity of NADH dehydrogenase and a reversed F1F0-
402 ATPase (Bruni and Kralj, 2020). Interestingly, while our study documented dysregulation in
403 membrane potential after gentamicin treatment, no significant differences were noted between
404 sensitive and tolerant strains. Despite prior research implicating increased survival of specific ATP
405 synthase knockouts in response to aminoglycoside treatments (Bruni and Kralj, 2020), our study
406 did not report a clear trend regarding the gentamicin tolerance of these knockout strains. We
407 acknowledge that variations in experimental conditions, such as medium composition, bacterial
408 strains, growth phase, treatment time, duration, and antibiotic compositions, may account for the
409 observed differences. Additionally, we recognize that genetic perturbations can have pleiotropic
410 effects, potentially altering cell survival and death mechanisms, which may differ from those
411 observed in the wild-type strain.

412 We conducted untargeted mass spectrometry to quantify proteins in the TCA-cycle and ETC
413 mutants. Utilizing the STRING database, we predicted functional protein interactions, revealing
414 significant enrichments in downregulated protein networks associated with ribosomal subunits,
415 translation factor activities, protein export mechanisms, and ribonucleoside monophosphate
416 biosynthesis in the mutant strains that displayed higher gentamicin tolerance. The altered levels of
417 ribosomal proteins observed in our mutant strains align well with a prior study that identified
418 respiratory complex I in *E. coli* as a critical mutational target for promoting persister cell formation
419 during the transition to a stationary phase (Van den Bergh et al., 2022). In that study, point
420 mutations in respiratory complex I, responsible for proton translocation, were found to induce
421 antibiotic tolerance (Van den Bergh et al., 2022). While they showed that mutations compromised

422 proton translocation, key components such as NADH oxidation, electron transfer, and drug uptake
423 remained largely unchanged (Van den Bergh et al., 2022). They also demonstrated that the
424 increased persistence correlated with an acidified cytoplasm during the stationary phase, impacting
425 protein translation and contributing to increased antibiotic tolerance, yet no significant differences
426 in pH and persistence were noted between mutant and wild-type strains during the exponential
427 phase (Van den Bergh et al., 2022). Similarly, our investigation revealed that single gene deletions
428 did not alter cellular PMF, redox activities, membrane potential, and drug uptake. However, the
429 downregulation of ribosomal protein levels reported in our study may not be attributed to a
430 reduction in cytoplasmic pH, as we did not observe alterations in pH levels in the knockout strains
431 compared to the wild type during the mid-exponential phase. Certain genes linked to the deletion
432 strains in our study, such as *icd, sucA, mdh,* and *fumA,* do not encode membrane-bound respiratory
433 proteins. Strain-specific differences can significantly influence the outcomes and responses to
434 various experimental conditions. Each strain of *E. coli* or any other microorganism can harbor
435 unique genetic backgrounds, mutation profiles, and physiological characteristics, leading to
436 distinct survival strategies in response to environmental stresses, such as antibiotic exposure.

437 In summary, our study revealed that deletions in TCA cycle and ETC genes, including *sucA, gltA,*
438 *mdh, sdhC, icd, acnB, fumA, nuoM,* and *nuoI*, increased aminoglycoside tolerance. Analyses,
439 including flow cytometry and proteomics, demonstrated enhanced tolerance without significant
440 changes in energy-dependent drug uptake or membrane potential. Our pathway analysis identified
441 a downregulation in large and small ribosomal binding proteins, ribosome biogenesis, translation
442 factor activity, and ribonucleoside monophosphate biosynthesis in all mutant strains, offering a
443 plausible explanation for the observed aminoglycoside tolerance in these mutants. Altogether, our
444 findings underscore the complexity of energy metabolism's role in antibiotic tolerance, providing
445 valuable insights into the molecular mechanisms of aminoglycoside tolerance in specific mutant
446 strains.

447

448 **MATERIALS AND METHODS**

449 **Bacterial strains, chemicals, media, and growth conditions**

450 We employed the in-house *Escherichia coli* K-12 MG1655 strain for our experiments. The gene
451 deletions in *E. coli* K-12 MG1655 were established in our prior studies(Ngo et al., n.d.) utilizing

452 the Datsenko and Wanner method (Datsenko and Wanner, 2000). *E. coli* K-12 BW25113 and its
453 corresponding knockout strains were procured from the Keio collection, purchased from Horizon
454 Discovery (Catalog #OEC4988, Lafayette, CO, USA). The validity of all deletions was confirmed
455 through the use of check primers (Ngo et al., n.d.). All chemicals utilized in the study were
456 purchased from Fisher Scientific (Atlanta, GA) or VWR International (Pittsburg, PA) unless stated
457 otherwise. The Gentamicin-Texas Red Conjugate (Catalog # 24300) was purchased from AAT
458 Bioquest, Inc (CA, USA). The ATP measurement kit (G8230) was acquired from Promega
459 Corporation (Madison, WI). Standard Luria-Bertani (LB) broth was prepared by dissolving 5 g
460 yeast extract, 10 g tryptone, and 10 g sodium chloride in 1 l of deionized (DI) water. LB agar was
461 made by dissolving 40 g of pre-mixed LB agar powder in 1 l DI water. Sterilization of LB broth
462 and LB agar was done via autoclaving at 121°C and 103.421 kPa. To determine tolerant cells in
463 cultures, gentamicin (50 μg/mL), streptomycin (50 μg/mL), and amikacin (50 μg/mL) were used,
464 and their concentrations were selected to be much higher than the minimum inhibitory
465 concentrations (MICs). MICs of antibiotics for *E. coli* were determined using MIC Test strips
466 (Fisher Scientific), as previously described (Andrews, 2001), and the results were presented in
467 **Supplementary Table S1**. Ampicillin (100 μg/mL) was utilized to maintain plasmids in the cells.
468 0.2% L-arabinose at 13.3 mM was added to the media to induce GFP expression. To decrease the
469 antibiotic concentration below the MIC, a sterile 1X phosphate buffer saline (PBS) solution was
470 utilized to wash the cells. Antibiotics were dissolved in DI water and sterilized using a 0.2 μm PES
471 syringe filter. Overnight cultures were prepared in 14 ml round-bottom tubes (Catalog # 14-959-
472 1B, Fisher Scientific) by incubating cells from a frozen 25% glycerol stock (-80°C) in 2 ml of LB
473 at 37°C and 250 rpm. After 24 hours, cells from the overnight cultures were diluted 1:100 fold in
474 2 ml of fresh medium and cultured further to achieve the desired growth phase for the assays.

475 **Cell growth assay**

476 To prepare overnight precultures, cells from frozen stocks were inoculated into 2 mL of LB
477 medium in 14-mL round-bottom tubes and cultured for 24 hours at 37°C with shaking at 250 rpm.
478 The overnight precultures were then diluted 100-fold in 14-mL round-bottom tubes containing 2
479 mL of LB medium and incubated in the shaker at 250 rpm and 37°C. The growth of the cultures
480 was determined by measuring the number of cells per mL using flow cytometry. To perform this
481 task, cells were transferred to PBS at specified time points and analyzed with a flow cytometer
482 (NovoCyte Flow Cytometer, NovoCyte 3000RYB, ACEA Biosciences Inc., San Diego, CA). The

483 cell populations were delineated on flow diagrams utilizing the forward and side scatter
484 parameters, with controls including PBS with cells and PBS without cells. The inclusion of a PBS
485 solution without cells aids in noise determination. The instrument is capable of quantifying both
486 the number of events and the volume of the solution under analysis. Roughly 30,000-50,000 events
487 were analyzed for each sample.

488 **Clonogenic survival assay**

489 Overnight cultures were prepared in 14 ml tubes by incubating cells from a frozen 25% glycerol
490 stock (-80°C) in 2 ml of LB at 37°C and 250 rpm. After 24 hours, cells from the overnight cultures
491 were diluted 1:100 fold in 2 ml of fresh medium and cultured in the incubator at 37°C with shaking.
492 At the designated growth phase or time points, cells were exposed to antibiotics at the specified
493 concentrations (50 µg/ml) for a duration of 5 hours. To determine the number of live cells before
494 antibiotic exposure, 10 µl of cell cultures were serially diluted in PBS and plated on an LB agar
495 plate, which was incubated for 16 hours at 37°C. During the antibiotic treatments, 1 ml cultures
496 were collected after 5 hours and washed twice with PBS through centrifugation at 13,300 rpm
497 (17,000 g) for 3 minutes to remove antibiotics. After the final centrifugation, 900 µl of supernatant
498 was removed using a pipette, and the cell pellets were resuspended in the remaining 100 µl of PBS.
499 Next, 10 µl of the cell suspensions were serially diluted in PBS, and 10 µl of the diluted cell
500 suspensions were spotted onto LB agar plates. The plates were then incubated at 37°C for at least
501 16 hours, and the colony-forming units (CFU) were counted to determine the number of live cells
502 present in the cultures. Survival fractions were calculated by dividing the number of surviving
503 cells (after treatment) by the initial number of cells (before treatment).

504 **Redox sensor green dye staining**

505 To measure bacterial reductase and ETC (electron transport chain) activities, we used the *Bac*Light
506 Redox Sensor Green Vitality kit (Catalog#B34954, Thermo Fisher) following the manufacturer's
507 instructions. Overnight cultures were prepared in 14 ml Falcon tubes by incubating cells from a
508 frozen 25% glycerol stock (-80°C) in 2 ml of LB at 37°C and 250 rpm. After 24 hours, cells from
509 the overnight cultures were diluted 1:100 fold in 2 ml of fresh medium and cultured in the incubator
510 at 37°C with shaking. For analyzing the cell populations during mid-exponential and early
511 stationary phases (t = 3h, 4h, 5h, 6h), we diluted the cells in 1 ml of 0.85% sodium chloride solution
512 in flow cytometry tubes (5 ml round bottom falcon tubes) by varying amounts (10-, 20-, 20-, 50-

513 fold, respectively). After that, Redox Sensor Green (RSG) dye was added to the cells at a
514 concentration of 1 μM, and the samples were incubated at 37°C for 10 minutes before flow
515 cytometry analysis. For the negative controls, cell suspensions were treated with 20 μM CCCP 5
516 minutes prior to RSG staining to disrupt membrane electron transport (**Supplementary Figure**
517 **S2**). Positive controls consisted of mid-exponential-phase cells. The cell populations were gated
518 on flow diagrams using the forward and side scatter parameters of unstained controls. Cells were
519 excited at 488 nm with a solid-state laser, and green fluorescence was collected with a 530/30
520 bandpass filter.

521 **ATP measurement**

522 The BacTiter-Glo Microbial Cell Viability assay kit (Catalog# G8230, Promega Corporation) was
523 used to measure the intracellular ATP levels of both *E. coli* MG1655 WT and mutant strains during
524 a specified growth phase, following the manufacturer's instructions. To generate a standard curve,
525 ATP solutions of known concentrations were used (**Supplementary Figure S2**). Background
526 luminescence was measured using LB broth.

527 **pH measurement**

528 For pH measurements in *E. coli*, a pGFPR01 plasmid was used, in which the GFP derivative
529 ratiometric pHluorin is expressed from the arabinose-induced promoter P_{BAD}. This plasmid was
530 kindly provided by Keith A. Martinez II (Department of Biology, Kenyon College, Gambier, Ohio,
531 USA). A comprehensive pH measurement protocol was obtained from a prior study (Van den
532 Bergh et al., 2022). Overnight cultures of WT and mutant strains were prepared in 14 ml tubes by
533 incubating cells carrying the pGFPR01 plasmid from a frozen 25% glycerol stock (-80°C) in 2 ml
534 of LB, 0.2% L-arabinose and 100 mg/ml ampicillin, at 37°C and 250 rpm. After 24 hours, cells
535 from the overnight cultures were diluted 1:100 fold in 2 ml of fresh medium, 0.2% L-arabinose
536 and 100 mg/ml ampicillin and cultured in the incubator at 37°C with shaking. Fluorescence was
537 measured at 410 nm and 470 nm using a plate reader at different time points, after measuring and
538 normalizing the optical density of cells in liquid culture. The 410/470 fluorescence ratios were
539 recorded to determine the cytoplasmic pH using the standard curve (**Supplementary Figure S3**).
540 To generate standard pH versus fluorescence ratio curves for *E. coli* MG1655 cells, transmembrane
541 pH was collapsed by adding 40 mM potassium benzoate and 40 mM methylamine hydrochloride
542 to the cells, equalizing the difference between the external and internal pH. The cultures were then

543 buffered to different pH levels ranging from 5 to 10 using a 50 mM concentration of 2-(*N*-
544 morpholino) ethanesulfonic acid (MES) or 3-(*N*-morpholino) propanesulfonic acid (MOPS), and
545 corresponding fluorescence values at 410 nm and 470 nm were obtained using a plate reader. The
546 Boltzmann equation was used to establish the standard curve for each bacterial strain based on the
547 provided data (Martinez II et al., 2012).

548 **$DiSC_3(5)$ assay**

549 The fundamental mechanism of this assay and the assessment of PMF components using $DiSC_3(5)$
550 have been extensively detailed elsewhere (Farha et al., 2013; Panta and Doerrler, 2021; Stokes et
551 al., 2020). *E. coli* MG1655 wild-type and mutant cells in both exponential and early stationary
552 phases (at time points t = 3 h, 4h, 5h, 6h) were collected and subjected to two washes with an assay
553 buffer containing 5 mM HEPES and 20 mM glucose. The cell density was set to OD_{600}=0.1, and
554 the cells were stained with 1 μM $DiSC_3(5)$. Fluorescence readings were taken at specified intervals
555 using a plate reader, with excitation and emission wavelengths set at 620 nm and 670 nm,
556 respectively. Gentamicin (50 μg/mL) was introduced 20 minutes after cells reached equilibrium.
557 At this point, the probe was released into the medium, leading to an upsurge in fluorescence. CCCP
558 (100 μM) and polymyxin B (32 μg/mL) were included as controls and administered 20 minutes
559 after equilibrium to dissipate the proton and electron gradients of PMF, respectively. The
560 concentration of polymyxin B at 32 μg/mL was determined based on a prior study (Stokes et al.,
561 2020).

562 **Gentamicin uptake assay**

563 Overnight cultures were prepared in 14 ml tubes by incubating cells from a frozen 25% glycerol
564 stock (-80°C) in 2 ml of LB at 37°C and 250 rpm. After 24 hours, cells from the overnight cultures
565 were diluted 1:100 fold in 2 ml of fresh medium and cultured in the incubator at 37°C with shaking.
566 At the mid-exponential phase (t=3.5 h), 100 μl of cell cultures for both wild-type and mutants were
567 exposed to gentamicin-Texas red (GTTR) at a final concentration of 25 μg/ml. Untreated mid-
568 exponential phase cells were used as negative controls. The samples containing gentamicin-Texas
569 red were then incubated for 1 hour at 37°C with shaking at 250 rpm. Subsequently, 20 μl from
570 each sample was washed with 500 μl of PBS (1X). After the final washing step, cell pellets were
571 resuspended in 500 μl of PBS. All samples were subjected to analysis using a flow cytometer

572 equipped with lasers emitting light at a wavelength of 561 nm, and the resulting red fluorescence
573 was detected using a 615/20 nm bandpass filter.

574 **Proteomics sample preparation and analysis**

575 Cells from both wild-type and mutant strains at the mid-exponential phase (t=3.5 h) were collected
576 after which protein extraction and digestion were carried out for Liquid Chromatography–Mass
577 Spectrometry (LC-MS) analysis by following the Sample Preparation by Easy Extraction and
578 Digestion (SPEED) procedure. The experiments were conducted at the University of Houston
579 Mass Spectrometry Laboratory under a service fee. Comprehensive details regarding the protein
580 isolation and digestion methods can be found elsewhere (Doellinger et al., 2020). Briefly, cell
581 pellets were added 20 uL TFA and incubated at room temperature for 5 min followed by addition
582 of 200 ul of 2M trisbase. After adding Tris(2-carboxyethyl) phosphine (10 mM) and 2-
583 Chloroacetamide (40 mM), the reaction mixture was heated at 95C for 5 min. Digestion was
584 performed by adding trypsin (1/40, w/w) and incubation at 37 ºC overnight. The digested peptides
585 were cleaned up using a C18 Ziptip and vacuum dried using a CentriVap (Labconco). Each dried
586 sample was resuspended in 2% ACN with 0.1% FA for LC-MS analysis. The method involving
587 LC-MS has been detailed in a separate publication (Qin et al., 2022). Specifically, a NanoElute
588 LC system connected to a timsTOF Pro (Bruker Daltonics, Germany) through a CaptiveSpray
589 source was utilized. Samples were loaded onto an in-house packed column (75 µm x 20 cm, 1.9
590 µm ReproSil-Pur C18 particle from Dr. Maisch GmbH, Germany) with a column temperature of
591 40 °C. Mobile phases included buffer A (0.1% FA in water) and buffer B (0.1% FA in ACN). The
592 short gradient was 0-17.8 minutes, from 2% B to 30% B, followed by 18.3 minutes to 95% B, and
593 20.7 minutes to 95% B. The parallel accumulation-serial fragmentation (PASEF) mode with 4
594 PASEF scans per cycle was employed. The electrospray voltage was set at 1.4 kV, and the ion
595 transfer tube temperature was maintained at 180 °C. Full MS scans were conducted across the
596 mass-to-charge (m/z) range of 150–1700. The target intensity value was 2.0×10^5 with a threshold
597 of 2500. A fixed cycle time of 0.53 s was established, and a dynamic exclusion duration of 0.4
598 minutes with a ± 0.015 amu tolerance was applied. Only peaks with a charge state of ≥ 2 were
599 chosen for fragmentation. The default settings of MSFragger (Yu et al., 2020) were applied to
600 analyze data obtained from the mentioned instrument. The UniProt-SwissProt *E. coli* K12 database
601 (Taxon ID 83333, downloaded on 6/19/2023, 4518 entries) served as the reference. Fixed
602 modification involved cysteine carbamidomethylation, while variable modifications included

603 methionine oxidation and acetylation. Peptide length was restricted to 7-50, allowing for 2 missed
604 cleavages. Both precursor and product ion masses were set as monoisotopic. The false discovery
605 rate (FDR) was controlled at <1% at the peptide spectrum match, peptide, and protein levels.

606 **Proteomics data analysis**

607 The processing of proteomics data and the calculations of fold change were essentially carried out
608 following the methods described in the paper by Aguilan *et al* (Aguilan et al., 2020). In summary,
609 we utilized Excel spreadsheets for key stages of data transformation, normalization, fold change,
610 and P-value calculation. Initially, proteins lacking quantitative values were excluded, and a
611 logarithm transformation was applied to achieve a normal distribution of data. Normalization,
612 using both average and slope methods, was then employed to minimize intragroup variation in
613 technical replicates and log fold change calculations compared to the transformed unnormalized
614 data. Subsequently, missing values were imputed by replacing them with approximated values
615 using the Probabilistic Minimum Imputation method. Following imputation, we determined the
616 relative ratio of each protein in mutant and wild-type strains, along with P-value calculation using
617 the parametric *t*-test. The selection of the *t*-test type involved an *F*-test to evaluate whether the
618 replicates for each protein exhibited homoscedastic (equal variances) or heteroscedastic (unequal
619 variances) characteristics. For the identification of significant networks among input proteins, we
620 utilized the STRING tool V 12.0. This entailed inputting proteins that were significantly
621 upregulated and downregulated based on specified thresholds, as detailed elsewhere (Szklarczyk
622 et al., 2023).

623 **Statistical analysis**

624 All assays were conducted using at least three independent biological replicates. The figures
625 display the mean value and standard error for each data point. Statistical analysis was performed
626 using GraphPad Prism software, with one-way analysis of variance (ANOVA) with Dunnett's post
627 hoc test to determine significance. The P value threshold was set at *, $P < 0.05$, **, $P < 0.01$, ***,
628 $P < 0.001$, ****, $P < 0.0001$, and ns nonsignificant.

629

630

631

632 **REFERENCES**

633

634 Aggen JB, Armstrong ES, Goldblum AA, Dozzo P, Linsell MS, Gliedt MJ, Hildebrandt DJ,
635 Feeney LA, Kubo A, Matias RD, Lopez S, Gomez M, Wlasichuk KB, Diokno R, Miller GH,
636 Moser HE. 2010. Synthesis and spectrum of the neoglycoside ACHN-490. *Antimicrob Agents*
637 *Chemother* **54**:4636–4642. DOI: https://doi.org/10.1128%2FAAC.00572-10, PMID:
638 20805391
639 Aguilan JT, Kulej K, Sidoli S. 2020. Guide for protein fold change and: P-value calculation for
640 non-experts in proteomics. *Mol Omics* **16**:573–582. DOI:
641 https://doi.org/10.1039/D0MO00087F, PMID: 32968743
642 Allison KR, Brynildsen MP, Collins JJ. 2011. Metabolite-enabled eradication of bacterial
643 persisters by aminoglycosides. *Nature* **473**:216–220. DOI:
644 https://doi.org/10.1038/nature10069, PMID: 21562562
645 Amato SM, Orman MA, Brynildsen MP. 2013. Metabolic Control of Persister Formation in
646 Escherichia coli. *Mol Cell* **50**:475–487. DOI: https://doi.org/10.1016/j.molcel.2013.04.002,
647 PMID: 23665232
648 Andrews JM. 2001. Determination of minimum inhibitory concentrations. *Journal of*
649 *Antimicrobial Chemotherapy* **48**:5–16. DOI: https://doi.org/10.1093/jac/48.suppl_1.5,
650 PMID: 11420333
651 Balaban NQ, Helaine S, Lewis K, Ackermann M, Aldridge B, Andersson DI, Brynildsen MP,
652 Bumann D, Camilli A, Collins JJ, Dehio C, Fortune S, Ghigo JM, Hardt WD, Harms A,
653 Heinemann M, Hung DT, Jenal U, Levin BR, Michiels J, Storz G, Tan MW, Tenson T, Van
654 Melderen L, Zinkernagel A. 2019. Definitions and guidelines for research on antibiotic
655 persistence. *Nat Rev Microbiol* **17**:441–448. DOI: https://doi.org/10.1038/s41579-019-0196-
656 3, PMID: 30980069
657 Becker B, Cooper MA. 2013. Aminoglycoside antibiotics in the 21st century. *ACS Chem Biol*
658 **8**:105–115. DOI: https://doi.org/10.1021/cb3005116, PMID: 23110460
659 Binder S, Levitt AM, Sacks JJ, Hughes JM. 1999. Emerging Infectious Diseases: Public Health
660 Issues for the 21st Century. *Science (1979)* **284**:1311–1313. DOI:
661 https://doi.org/10.1126/science.284.5418.1311, PMID: 10334978
662 Borovinskaya MA, Pai RD, Zhang W, Schuwirth BS, Holton JM, Hirokawa G, Kaji H, Kaji A,
663 Cate JHD. 2007. Structural basis for aminoglycoside inhibition of bacterial ribosome
664 recycling. *Nat Struct Mol Biol* **14**:727–732. DOI: https://doi.org/10.1038/nsmb1271, PMID:
665 17660832
666 Bruni GN, Kralj JM. 2020. Membrane voltage dysregulation driven by metabolic dysfunction
667 underlies bactericidal activity of aminoglycosides. *Elife* **9**:1–25. DOI:
668 https://doi.org/10.7554/eLife.58706, PMID: 32748785
669 Datsenko KA, Wanner BL. 2000. One-step inactivation of chromosomal genes in Escherichia coli
670 K-12 using PCR products. *PNAS* **97**:6640–6645. DOI:
671 https://doi.org/10.1073/pnas.120163297, PMID: 10829079
672 Davis BD, Chen L, Tai PC. 1986. Misread protein creates membrane channels: An essential step
673 in the bactericidal action of aminoglycosides. *PNAS* **83**:6164–6168. DOI:
674 https://doi.org/10.1073/pnas.83.16.6164, PMID: 2426712
675 Doellinger J, Schneider A, Hoeller M, Lasch P. 2020. Sample preparation by easy extraction and
676 digestion (SPEED) - A universal, rapid, and detergent-free protocol for proteomics based on

677 acid extraction. *Molecular and Cellular Proteomics* **19**:209–222. DOI:
678 https://doi.org/10.1074/mcp.tir119.001616, PMID: 31754045
679 Domingues MM, Inácio RG, Raimundo JM, Martins M, Castanho MARB, Santos NC. 2012.
680 Biophysical characterization of polymyxin B interaction with LPS aggregates and membrane
681 model systems. *Biopolymers* **98**:338–344. DOI: https://doi.org/10.1002/bip.22095, PMID:
682 23193598
683 Endimiani A, Hujer KM, Hujer AM, Armstrong ES, Choudhary Y, Aggen JB, Bonomo RA. 2009.
684 ACHN-490, a neoglycoside with potent in vitro activity against multidrug-resistant Klebsiella
685 pneumoniae isolates. *Antimicrob Agents Chemother* **53**:4504–4507. DOI:
686 https://doi.org/10.1128%2FAAC.00556-09, PMID: 19770287
687 Farha MA, Verschoor CP, Bowdish D, Brown ED. 2013. Collapsing the proton motive force to
688 identify synergistic combinations against Staphylococcus aureus. *Chem Biol* **20**:1168–1178.
689 DOI: https://doi.org/10.1016/j.chembiol.2013.07.006, PMID: 23972939
690 Germain E, Roghanian M, Gerdes K, Maisonneuve E. 2015. Stochastic induction of persister cells
691 by HipA through (p)ppGpp-mediated activation of mRNA endonucleases. *Proc Natl Acad*
692 *Sci U S A* **112**:5171–5176. DOI: https://doi.org/10.1073/pnas.1423536112, PMID: 25848049
693 Guo H, Suzuki T, Rubinstein JL. 2019. Structure of a bacterial ATP synthase. *Elife* **8**:e43128. DOI:
694 https://doi.org/10.7554/eLife.43128, PMID: 30724163
695 Kohanski MA, Dwyer DJ, Hayete B, Lawrence CA, Collins JJ. 2007. A Common Mechanism of
696 Cellular Death Induced by Bactericidal Antibiotics. *Cell* **130**:797–810. DOI:
697 https://doi.org/10.1016/j.cell.2007.06.049, PMID: 17803904
698 Kohanski MA, Dwyer DJ, Wierzbowski J, Cottarel G, Collins JJ. 2008. Mistranslation of
699 Membrane Proteins and Two-Component System Activation Trigger Antibiotic-Mediated
700 Cell Death. *Cell* **135**:679–690. DOI: https://doi.org/10.1016/j.cell.2008.09.038, PMID:
701 19013277
702 Krause KM, Serio AW, Kane TR, Connolly LE. 2016. Aminoglycosides: An overview. *Cold*
703 *Spring Harb Perspect Med* **6**. DOI: https://doi.org/10.1101/cshperspect.a027029, PMID:
704 27252397
705 Kresge N, Simoni RD, Hill RL. 2004. Selman Waksman: the Father of Antibiotics. *Journal of*
706 *Biological Chemistry* **279**:e7–e8. DOI: https://doi.org/10.1016/s0021-9258(20)67861-9
707 Lambert PA. 2005. Bacterial resistance to antibiotics: Modified target sites. *Adv Drug Deliv Rev*
708 **57**:1471–1485. DOI: https://doi.org/10.1016/j.addr.2005.04.003, PMID: 15964098
709 Landman D, Babu E, Shah N, Kelly P, Bäcker M, Bratu S, Quale J. 2010. Activity of a novel
710 aminoglycoside, ACHN-490, against clinical isolates of Escherichia coli and Klebsiella
711 pneumoniae from New York City. *Journal of Antimicrobial Chemotherapy* **65**:2123–2127.
712 DOI: https://doi.org/10.1093/jac/dkq278, PMID: 20667885
713 Martinez II KA, Kitko RD, Mershon JP, Adcox HE, Malek KA, Berkmen MB, Slonczewski JL.
714 2012. Cytoplasmic pH Response to Acid Stress in Individual Cells of Escherichia coli and
715 Bacillus subtilis Observed by Fluorescence Ratio Imaging Microscopy. *Appl Environ*
716 *Microbiol* **78**:3706–3714. DOI: https://doi.org/10.1128/AEM.00354-12, PMID: 22427503
717 Miesenböck G, Angelis DA De, Rothman JE. 1998. Visualizing secretion and synaptic
718 transmission with pH-sensitive green fluorescent proteins. *Nature* **394**:192–195. DOI:
719 https://doi.org/10.1038/28190, PMID: 9671304
720 Moazed D, Noller HF. 1987. Interaction of antibiotics with functional sites in 16S ribosomal RNA.
721 *Nature* **327**:389–394. DOI: https://doi.org/10.1038/327389a0, PMID: 2953976

722 Mohiuddin SG, Kavousi P, Orman MA. 2020. Flow-cytometry analysis reveals persister
723 resuscitation characteristics. *BMC Microbiol* **20**:1–13. DOI: https://doi.org/10.1186/s12866-
724 020-01888-3, PMID: 32640993
725 Mohiuddin SG, Massahi A, Orman MA. 2022. High-Throughput Screening of a Promoter Library
726 Reveals New Persister Mechanisms in Escherichia Coli. *Microbiol Spectr* **10**:e02253-21.
727 DOI: https://doi.org/10.1128/spectrum.02253-21, PMID: 35196813
728 Molina-Quiroz RC, Silva-Valenzuela C, Brewster J, Castro-Nallar E, Levy SB, Camilli A. 2018.
729 Cyclic AMP Regulates Bacterial Persistence through Repression of the Oxidative Stress
730 Response and SOS-Dependent DNA Repair in Uropathogenic Escherichia coli. *mBio*
731 **9**:e02144-17. DOI: https://doi.org/10.1128/mBio.02144-17, PMID: 29317513
732 Ngo HG, Mohiuddin SG, Ananda A, Orman MA. 2023. Unraveling Crp/cAMP-Mediated
733 Metabolic Regulation in Antibiotic-Tolerant Cells of *Escherichia coli*. Under Review.
734 Okusu H, Ma D, Nikaido H. 1996. AcrAB Efflux Pump Plays a Major Role in the Antibiotic
735 Resistance Phenotype of Escherichia coli Multiple-Antibiotic-Resistance (Mar) Mutants. *J*
736 *Bacteriol* **178**:306–308. DOI: https://doi.org/10.1128/jb.178.1.306-308.1996, PMID:
737 8550435
738 Panta PR, Doerrler WT. 2021. A Burkholderia thailandensis DedA Family Membrane Protein Is
739 Required for Proton Motive Force Dependent Lipid A Modification. *Front Microbiol*
740 **11**:618389. DOI: https://doi.org/10.3389/fmicb.2020.618389, PMID: 33510730
741 Qin G, Zhang P, Sun M, Fu W, Cai C. 2022. Comprehensive spectral libraries for various rabbit
742 eye tissue proteomes. *Sci Data* **9**:111. DOI: https://doi.org/10.1038/s41597-022-01241-5,
743 PMID: 35351915
744 Recht MI, Douthwaite S, Dahlquist KD, Puglisi JD. 1999. Effect of Mutations in the A Site of 16
745 S rRNA on Aminoglycoside Antibiotic-Ribosome Interaction. *J Mol Biol* **286**:33–43. DOI:
746 https://doi.org/10.1006/jmbi.1998.2446, PMID: 9931247
747 Ristuccia AM, Cunha BA. 1985. An overview of amikacin. *Ther Drug Monit* **7**:12–25. DOI:
748 https://doi.org/10.1097/00007691-198503000-00003, PMID: 3887667
749 Schatz A, Bugie E, Waksman SA. 2005. Streptomycin, a substance exhibiting antibiotic activity
750 against gram-positive and gram-negative bacteria. 1944. *Clin Orthop Relat Res* **437**:3–6.
751 DOI: https://doi.org/10.1097/01.blo.0000175887.98112.fe, PMID: 16056018
752 Stokes JM, Yang K, Swanson K, Jin W, Cubillos-Ruiz A, Donghia NM, MacNair CR, French S,
753 Carfrae LA, Bloom-Ackerman Z, Tran VM, Chiappino-Pepe A, Badran AH, Andrews IW,
754 Chory EJ, Church GM, Brown ED, Jaakkola TS, Barzilay R, Collins JJ. 2020. A Deep
755 Learning Approach to Antibiotic Discovery. *Cell* **180**:688-702.e13. DOI:
756 https://doi.org/10.1016/j.cell.2020.01.021, PMID: 32084340
757 Szklarczyk D, Gable AL, Lyon D, Junge A, Wyder S, Huerta-Cepas J, Simonovic M, Doncheva
758 NT, Morris JH, Bork P, Jensen LJ, Von Mering C. 2019. STRING v11: Protein-protein
759 association networks with increased coverage, supporting functional discovery in genome-
760 wide experimental datasets. *Nucleic Acids Res* **47**:D607–D613. DOI:
761 https://doi.org/10.1093/nar/gky1131, PMID: 30476243
762 Szklarczyk D, Kirsch R, Koutrouli M, Nastou K, Mehryary F, Hachilif R, Gable AL, Fang T,
763 Doncheva NT, Pyysalo S, Bork P, Jensen LJ, Von Mering C. 2023. The STRING database in
764 2023: protein-protein association networks and functional enrichment analyses for any
765 sequenced genome of interest. *Nucleic Acids Res* **51**:D638–D646. DOI:
766 https://doi.org/10.1093/nar/gkac1000, PMID: 36370105

767 Taber Harry W, Mueller JP, Miller PF, Arrow AS. 1987. Bacterial Uptake of Aminoglycoside
768 Antibiotics. *Microbiol Rev* **51**:439–457. DOI: https://doi.org/10.1128/mr.51.4.439-457.1987,
769 PMID: 3325794
770 Theodore A, Lewis K, Vulić M. 2013. Tolerance of Escherichia coli to fluoroquinolone antibiotics
771 depends on specific components of the SOS response pathway. *Genetics* **195**:1265–1276.
772 DOI: https://doi.org/10.1534/genetics.113.152306, PMID: 24077306
773 Van den Bergh B, Schramke H, Michiels JE, Kimkes TEP, Radzikowski JL, Schimpf J, Vedelaar
774 SR, Burschel S, Dewachter L, Lončar N, Schmidt A, Meijer T, Fauvart M, Friedrich T,
775 Michiels J, Heinemann M. 2022. Mutations in respiratory complex I promote antibiotic
776 persistence through alterations in intracellular acidity and protein synthesis. *Nat Commun*
777 **13**:546. DOI: https://doi.org/10.1038/s41467-022-28141-x, PMID: 35087069
778 Woodcock J, Moazed D, Cannon M, Davies J, Noller HF. 1991. Interaction of antibiotics with A-
779 and P-site-specific bases in 16S ribosomal RNA. *EMBO J* **1**:3099–3103. DOI:
780 https://doi.org/10.1002/j.1460-2075.1991.tb07863.x, PMID: 1915283
781 Woodruff HB. 2014. Selman A. Waksman, winner of the 1952 nobel prize for physiology or
782 medicine. *Appl Environ Microbiol* **80**:2–8. DOI: https://doi.org/10.1128/AEM.01143-13,
783 PMID: 24162573
784 Wu M, Maier E, Benz R, Hancock REW. 1999. Mechanism of interaction of different classes of
785 cationic antimicrobial peptides with planar bilayers and with the cytoplasmic membrane of
786 Escherichia coli. *Biochemistry* **38**:7235–7242. DOI: https://doi.org/10.1021/bi9826299,
787 PMID: 10353835
788 Yu F, Haynes SE, Teo GC, Avtonomov DM, Polasky DA, Nesvizhskii AI. 2020. Fast Quantitative
789 Analysis of timsTOF PASEF Data with MSFragger and IonQuant. *Molecular and Cellular*
790 *Proteomics* **19**:1575–1585. DOI: https://doi.org/10.1074/mcp.TIR120.002048, PMID:
791 32616513
792

793 **Data Availability**

794 The proteomics data will be submitted to one of the NIH-designated repositories. All data
795 generated or analyzed during this study have been incorporated into the manuscript and
796 supplemental files.

797 **Author Details**

798 Mehmet Orman

799 William A. Brookshire Department of Chemical and Biomolecular Engineering, University of
800 Houston

801 Contribution: Conceptualization, Data curation, Supervision, Funding acquisition, Investigation,
802 Writing - original draft, Project administration, Writing – review and editing

803 For correspondence: morman@central.uh.edu

Competing interests: No competing interests declared

Rauf Shiraliyev

William A. Brookshire Department of Chemical and Biomolecular Engineering, University of Houston

Contribution: Data curation, Investigation, Writing - original draft, review and editing

Competing interests: No competing interests declared

Acknowledgment

The authors would like to thank the members of Orman Lab for their help. This study was supported by NSF CAREER 2044375 and NIH/NIAID R01-AI143643.

Proteomics experiments were conducted at the Mass Spectrometry Laboratory of Dr. Chengzhi Cai at the University of Houston, with the associated service fees.